Electronic Supplementary Material (ESI) for Nanoscale.

Targeted modifications of monolithic multiterminal superconducting weak-links: Electronic Supplementary Information

Simon Collienne,*,† Danial Majidi,‡ Joris Van de Vondel,¶ Clemens B. Winkelmann,‡ and Alejandro V. Silhanek*,†

†*Experimental Physics of Nanostructured Materials, Q-MAT, CESAM, Université de Liège, B-4000 Sart Tilman, Belgium*

‡*Univ. Grenoble Alpes, CNRS, Grenoble INP, Institut Néel, 38000 Grenoble, France*

¶*Quantum Solid-State Physics, Department of Physics and Astronomy, KU Leuven, Celestijnenlaan 200D, B-3001 Leuven, Belgium*

E-mail: scollienne@uliege.be; asilhanek@uliege.be

Fabrication details

We fabricate the sample on a 2 inch double side polished sapphire substrate. Possessing a high thermal conductivity of sapphire, makes it highly suitable for our measurement where a fast thermal equilibrium is needed. First, a R-plane-oriented (1-102) sapphire substrate is transferred in the evaporation chamber of an ultra high vacuum electron (UHV) gun evaporator. Then, prior to 50 nm-thick Nb deposition, the substrate is heated at 660 °C to make oxygen contamination departing from the sapphire substrate.[1,2] The vacuum is kept lower that 10^{-9} Torr during Nb deposition. Eventually, in order to protect the Nb film from oxidation, a 5 nm-thick silicon capping layer is evaporated after letting the sample cool down below 80 °C in the same vacuum cycle. yTron devices are realized utilizing an Al hard mask on top of the Nb film by ebeam lithography and followed by lift-off procedure. The unprotected area of Nb with the Al mask is then removed by a reactive ion etching with a 20 W SF_6 plasma for 1 minute. Finally, the Al is removed by wet etching using the base developer MF319 for 3.5 minutes.

Finite elements model

In order to obtain the evolution of the temperature distribution during the reversible Joule heating regime, we performed finite element simulations. The model considers the sample as a thin film of 50 nm thickness whose exact geometry is obtained from scanning electron microscope (SEM) image. The spatial distributions of temperature and electric potential are calculated by solving the heat and continuity equations. The heat equation, is written :

$$\kappa \nabla^2 T + Q(T, \mathbf{r}) = 0 \tag{1}$$

with T the temperature in K and κ the thermal conductivity in $\mathrm{WK^{-1}m^{-1}}$. The last term in (1) is determined by the Joule heating $Q(T, \mathbf{r}) = \rho(T)\mathbf{J}^2(\mathbf{r})$ with $\rho(T) = \rho_0[1 + \alpha(T - T_0)]$ the temperature dependent electrical resistivity in Ωm. The parameter α is estimated from $R(T)$ measurements between 10 K and 300 K. The continuity equation is given by:

$$\nabla \cdot \mathbf{J} = 0 \tag{2}$$

where $\mathbf{J}(\mathbf{r})$ is the current density in $\mathrm{Am^{-2}}$. Finally, the Ohm's law $\mathbf{E} = \rho(T)\mathbf{J}$ and the electrical field $\mathbf{E} = -\nabla V$ complete the system of equations. The parameters used in the simulations are summarized in Table S1.

Table S1: Thermal conductivity, electrical resistivity and thermal coefficient as input parameters in COMSOL simulations.

	κ ($\mathrm{WK^{-1}m^{-1}}$)	ρ ($\mu\Omega$cm)	α ($\mathrm{K^{-1}}$)
Nb	5	1.33	8×10^{-3}
Sapphire	3	/	/

The main panel of Fig. S1 shows the evolution of the resistance (R) as a function of the applied current (I) at the bath temperature $T_b = 10$ K. The observed parabolic profile typical of Joule heating is followed by a important resistance increase associated to structural modification caused by electroannealing. It is precisely in this high-currents regime

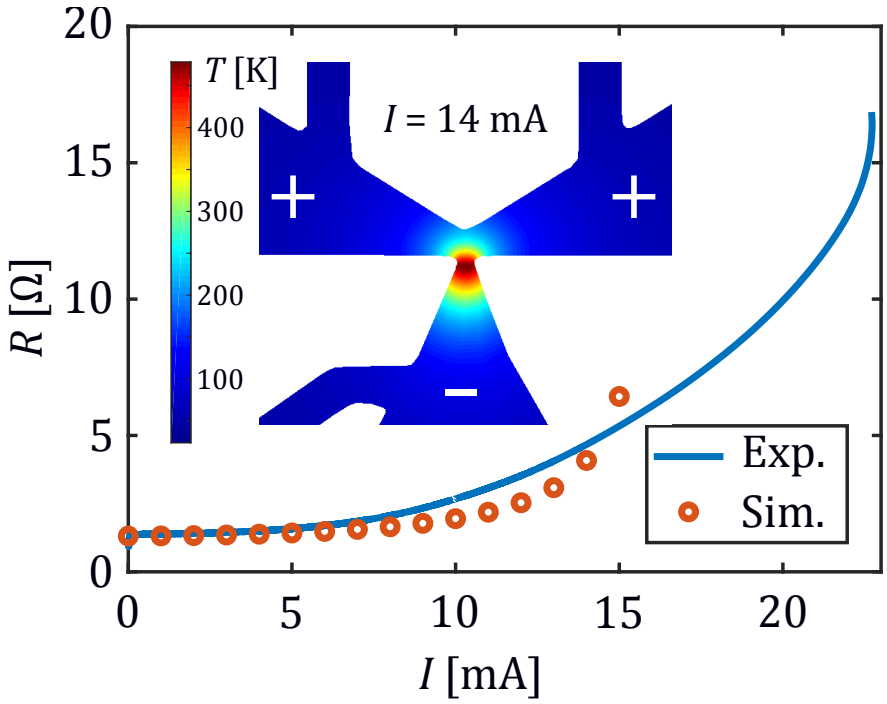

Figure S1: Typical curve of an EA experiment (blue line) and the result of the finite element model for some values of bias current (red circles). The inset shows the obtained temperature map for I = 14 mA with the given polarities.

that permanent modifications of the junctions lead to the irreversible modifications of the normal state resistance and critical current of the device (see Fig. 4 in the main text). The results of the simulations are represented by the red circles and allow us to estimate the temperature distribution in the sample for currents below 15 mA. The inset of Fig. S1 gives the temperature mapping for the special case $I = 14$ mA.

Atomic force microscopy imaging of the targeted structural modification

The high selectivity of the electroannealing process demonstrated at low temperatures through electric measurements (see main text) can be revealed by direct visualization under an atomic force microscope as shown in Fig. S2. These images were acquired in tapping mode and under ambient conditions. Panel (a) corresponds to the sample in its pristine state (i.e. before electroannealing). For this initial state, each junction is characterized by a resistance $R_i \sim 9.1\ \Omega$. Panel (b) shows the topography of the sample after targeted electroannealing at junction #2 with a current ~ 14 mA. A clear bump develops in the target junction with no evident modification taking place in the neighboring junctions. We speculate that the observed morphological change is due in part to oxygen up-take into the structure and the important oxygen diffusion in Nb above 400 K.[3] This observation is consistent with an increase of the resistance $R_2 = 33.6\,\Omega$ while the other resistances $R_1 \sim R_3 = 9.4\,\Omega$ remain nearly unaffected. Panel (c) shows a subsequent further modification on terminal 2 with $R_2 = 80\,\Omega$, with rather minor modifications on $R_1 = 9.4\,\Omega$ and $R_3 = 10.2\,\Omega$. It is worth noticing that the in this second electroannealing process, the propagating front of displaced matter does not advance further but instead hillocks appears on the sides of the junction #2.

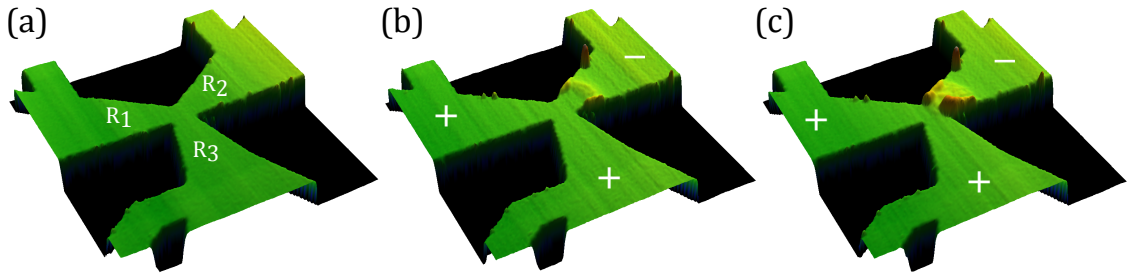

Figure S2: Atomic force microscopy image of (a) the sample in its initial state, and after targeted modification of the terminal 2 following the first (b) and second (c) electroannealing steps. The used polarities are indicated in the figure and are identical to that used at low temperatures.

We have also investigated the importance of the current polarity. The main results are summarized in Fig. S3. Panel (a) reproduces the results presented in panel (c) of Fig. S2. In this case, the transport of material flows away from the center of the device. In panel (b) we show that for opposite polarity the material displacement is reversed, i.e. towards the center of the device. Electric transport measurements confirm the observed current polarity effect. Indeed, for the case of Fig. S3(b), all three junction resistances are increased after EA and therefore the high selectivity obtained for the polarity shown in panel (a), is not verified when the polarity is reversed. We also observe the systematic formation of hillocks on the sides of junction #2 which can be explained by the high current density (panel (c)) and lower diffusion activation energy on the sample surface.

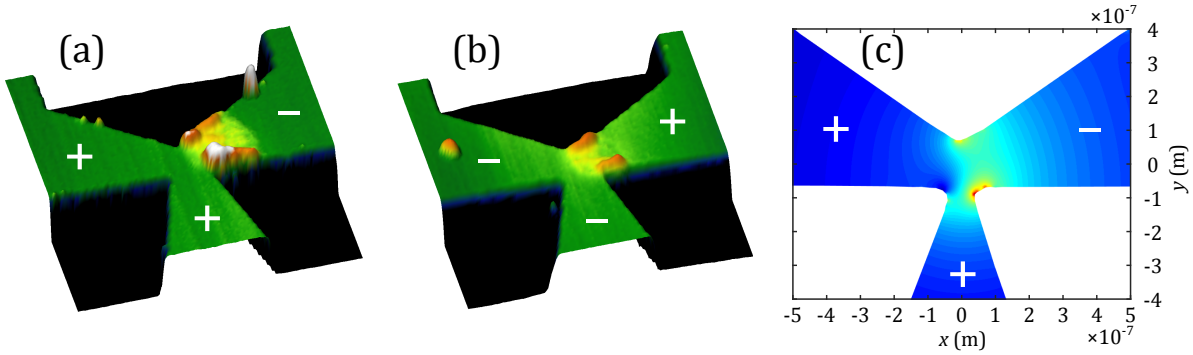

Figure S3: Atomic force microscopy image of (a) the sample with current bias as implemented in this work and with opposite polarity (b). Panel (c) shows the profile of current density norm which is valid for both panel (a) and (b).

References

1. Sürgers, C.; Löhneysen, H. v. Effect of oxygen segregation on the surface structure of single-crystalline niobium films on sapphire. *Appl.Phys. A* **1992**, *54*, 350–354.

2. Oya, G.; Koishi, M.; Sawada, Y. High-quality single-crystal Nb films and influences of substrates on the epitaxial growth. *J. Appl. Phys.* **1986**, *60*, 1440–1446.

3. Halbritter, J. On the oxidation and on the superconductivity of niobium. *Appl. Phys. A* **1987**, *43*, 1–28.